NANO LETTERS

Letter

pubs.acs.org/NanoLett

Gate-Controlled Surface Conduction in Na-Doped Bi_2Te_3 Topological Insulator Nanoplates

Yong Wang,*[,†,‡,§] Faxian Xiu,[∥] Lina Cheng,[§] Liang He,[‡] Murong Lang,[‡] Jianshi Tang,[‡] Xufeng Kou,[‡] Xinxin Yu,[‡] Xiaowei Jiang,[‡] Zhigang Chen,[§] Jin Zou,*[,§,⊥] and Kang L. Wang*[,‡]

[†]State Key Laboratory for Silicon Materials and Center for Electron Microscopy, Department of Materials Science and Engineering, Zhejiang University, Hangzhou, 310027, China

[‡]Department of Electrical Engineering, University of California, Los Angeles, California 90095, United States

[§]Division of Materials, The University of Queensland, Brisbane QLD 4072, Australia

[∥]Department of Electrical and Computer Engineering, Iowa State University, Ames, Iowa 50011, United States

[⊥]Centre for Microcopy and Microanalysis, The University of Queensland, Brisbane QLD 4072, Australia

Supporting Information

ABSTRACT: Exploring exciting and exotic physics, scientists are pursuing practical device applications for topological insulators. The Dirac-like surface states in topological insulators are protected by the time-reversal symmetry, which naturally forbids backscattering events during the carrier transport process, and therefore offers promising applications in dissipationless spintronic devices. Although considerable efforts have been devoted to controlling their surface conduction, limited work has been focused on tuning surface states and bulk carriers in Bi_2Te_3 nanostructures by external field. Here we report gate-tunable surface conduction in Na-doped Bi_2Te_3 topological insulator nanoplates. Significantly, by applying external gate voltages, such topological insulators can be tuned from p-type to n-type. Our results render a promise in finding novel topological insulators with enhanced surface states.

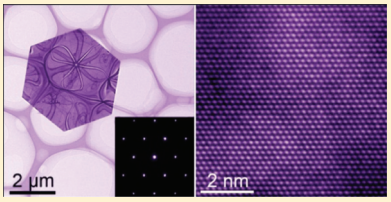

KEYWORDS: *Topological insulator, bismuth telluride, sodium doping, surface states, field-effect transistor*

In the past few years, topological insulators with both metallic surface states and insulating bulk states have attracted enormous attention due to their exotic physical properties and potential applications in low dissipation devices and quantum computing,[1−16] particularly after the experimental confirmation of a three-dimensional topological insulator.[17] These novel materials and related hybrid structures are expected to serve as a platform for creating and investigating some mysterious particles such as Axion and Majorana fermions, which have not yet been observed in experiments.[8] Protected by the time-reversal symmetry, the metallic surface states in topological insulators show a single Dirac cone at the Γ point in the energy dispersion spectrum, which excludes the backscattering induced by nonmagnetic impurities.[18] Extensive studies involving angle-resolved photoemission spectroscopy (ARPES), scanning tunneling microscopy, and transport measurements have confirmed the existence of such surface states in Bi_2Se_3,[11,19−21] Bi_2Te_3,[14,16,22,23] Sb_2Te_3,[19] and HgTe quantum well structures.[2]

Currently, topological insulator materials are generally produced by mechanical exfoliation,[16,24] molecular beam epitaxy[25,26] and chemical solutions synthesis.[14,27] However, no matter what growth method is employed, the resulting topological insulator materials share a common problem that the bulk contribution usually overwhelms the surface states because of the fact that the Fermi level usually lies in either valence band or conduction band due to the presence of intrinsic or extrinsic defects.[8,28,29] In order to resolve this problem, various approaches have been attempted to reduce the bulk conduction contribution and enhance that of the surface states, including elemental compensating doping[22,28,30,31] and electric gating.[14,32,33] Indeed, considerable progress has been made in terms of shifting the Fermi level (or the chemical potential) into the bulk band gap. However, most of these studies are focused on the photoelectron emission method by ARPES.[22,34] Using electric gating to tune the Fermi level has been realized in Bi_2Se_3[32,33,35] and in Bi_2Te_3.[14] For example, Steinberg et al.[33] swept the Fermi level across the Dirac point by applying double gating in a Bi_2Se_3 nanodevice. Likewise, by applying a back gate voltage to deplete the bulk carriers, we have previously achieved an enhanced surface conductance in a p-type Bi_2Te_3 nanoribbon at a positive bias of 80 V.[14] The surface states, however, could not be distinguished under zero and negative gate voltages due to the Fermi level falling into the valence band. The ideal scenario to maximize the surface contribution is to place the Fermi level right at the intrinsic Fermi level where the bulk contribution reaches the minimum.

In this work, by using a proper elemental doping, we revealed that the Fermi level of Bi_2Te_3 can be tuned by Na doping in

Received: August 22, 2011
Revised: February 5, 2012
Published: February 7, 2012

dx.doi.org/10.1021/nl202920p | *Nano Lett.* 2012, 12, 1170−1175

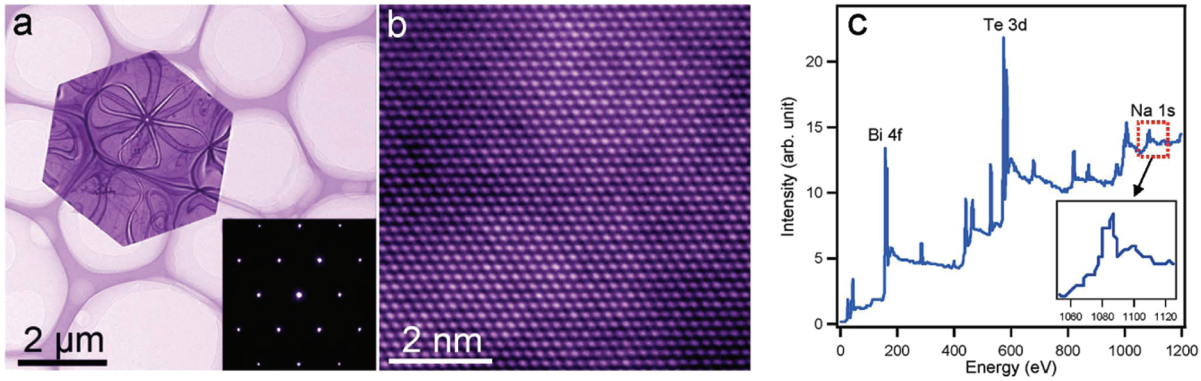

Figure 1. (a) Low-magnification TEM image of a Bi_2Te_3 nanoplate on a holey carbon grid. The inset is a selected area diffraction pattern taken along Bi_2Te_3 [0001] direction. Sharp diffraction spots indicate high-quality single-crystallinity. (b) A high-resolution TEM image taken along the Bi_2Te_3 [0001] direction, revealing a perfect crystalline structure. (c) A typical XPS profile shows the presence of Na in Bi_2Te_3. The concentration of Na was determined to be ~0.8%.

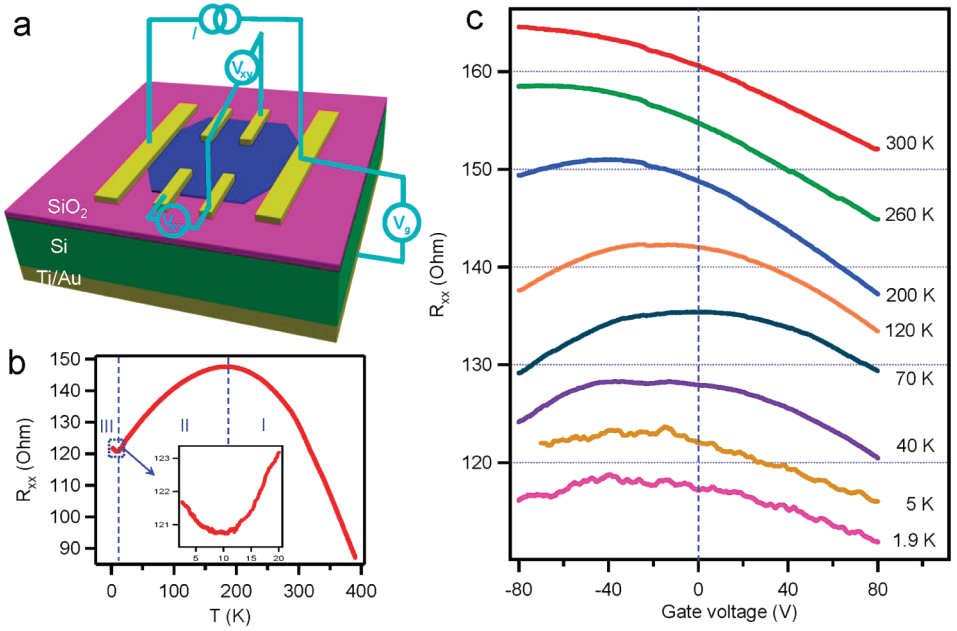

Figure 2. (a) A schematic drawing of a typical back-gate FET device. The nanoplate has a thickness of ~40 nm, and the channel length of ~1.2 μm. (b) Channel resistance as a function of temperature. Three different regions are identified. The inset shows an enlarged area marked by a dashed square in panel b. (c) Channel resistance as a function of gate voltage and temperature under zero magnetic field. Except for the curve at 1.9 K, all curves are vertically offset for clarity.

Bi_2Te_3 nanoplates, toward the middle of band gap. Taking these nanoplates as the conducting channels in field-effect transistor (FET) structures, we observed enhanced surface states in Bi_2Te_3 topological insulator nanoplates without applying a gate bias. Furthermore, by applying a back-gate voltage, we demonstrated the capability to tune the Na-doped Bi_2Te_3 nanoplates from p-type to n-type.

Sodium doped Bi_2Te_3 nanoplates were synthesized by solvothermal method. The detailed synthesis procedure is outlined as follows. First, high-purity polyvinyl pyrrolidone (PVP) was dissolved in ethylene glycol (40 mL) to form a clear solution, followed by the additions of Bi_2O_3 powders (0.5 mmol) and Te powders (1.5 mmol). The prepared solution was mixed by NaOH solution (5 mol/L) with a quantity of 2 mL. The resulting suspension was stirred vigorously for 30 min at 50−70 °C, and subsequently 0.2 g of $NaBH_4$ was added. The suspension was sealed in a 60 mL steel autoclave and then heated to 230−250 °C, maintaining for 24−48 h. The synthesized products were collected by a high-speed centrifugation, washed six times by the distilled water and absolute ethanol, and finally dried at 50 °C for 48 h in an oven.

Transmission electron microscopy (TEM) investigations were carried out on a Philips Tecnai F20 TEM operating at 200 kV to determine the structural characteristics of the synthesized Bi_2Te_3 nanoplates. A TEM image of a typical Bi_2Te_3 nanoplate is shown in Figure 1a, where a hexagonal-shaped nanoplate can be clearly identified. In general, the nanoplates are of 3−6 μm in lateral dimensions and 35−50 nm in thickness. The inset in Figure 1a is a selected-area electron diffraction pattern taken along the normal of the nanoplate, showing the single crystallinity of the nanoplate.[14,27] The high quality of the nanoplate is confirmed by the high-resolution TEM image (Figure 1b), where hexagonal lattice arrangements can be clearly observed, consistent with previous results.[14,27] X-ray photoelectron spectroscopy in a Perkin−Elmer PHI Model 560 XPS/Sam/SIMS I multitechnique surface analysis system

dx.doi.org/10.1021/nl202920p | Nano Lett. 2012, 12, 1170−1175

was applied to study the composition of the synthesized nanoplates and the result is shown in Figure 1c, where Bi, Te, Na can be easily identified.[36] From the results in Figure 1c, a percentage of ~0.8% Na in the Bi_2Te_3 nanoplates is determined.

To investigate the transport properties and explore the surface states in the Na doped Bi_2Te_3 nanoplates, back-gate FET devices with a standard six-terminal Hall-bar geometry were fabricated, as schematically illustrated in Figure 2a (see Figure S1 for the optical image and the detailed information of the fabricated device in the Supporting Information). The longitudinal resistance (R_{xx}) as a function of the temperature (T), that is, the $R_{xx}-T$ plot, is displayed in Figure 2b, where three different regimes (marked by I, II, and III) can be clearly distinguished. In regime I (~185−390 K), the channel resistance decreases with increased temperature, showing a semiconducting-like behavior;[37] in regime II (~10−185 K), the $R_{xx}-T$ plot shows a typical metallic behavior as the resistance rises with the temperature where phonon scattering dominates;[14] in regime III (2−10 K, enlarged in the inset), the resistance starts to rise again when the temperature approaches 10 K, which can be ascribed to the carrier freeze-out effect, as reported in Bi_2Te_3 nanoribbons.[14] The observed $R_{xx}-T$ curve of Na-doped Bi_2Te_3 nanoplates is similar to those appeared in Sb doped Bi_2Se_3 where a low carrier density was obtained,[37] while it is different from the Bi_2Te_3 nanoribbons where metallic behavior dominate at high temperature.[14] It should be noted that the conductance of the nanoplate system consists of multiple conduction channels, involving bulk and surface channels (confirmed later). Therefore, it is not likely to extract the activation energy from the Regimes I and III through curve-fitting of the $R_{xx}-T$ plot (Supporting Information, Figure S2).[14]

Figure 2c shows the channel resistance as a function of the gate voltage (V_g) at various temperatures for the Bi_2Te_3-based FET. It is of interest to note that the gate modulated resistance exhibits distinct behaviors at different temperatures. At 300 K, the resistance decreases with increasing the gate voltage, showing a clear n-type feature. When the temperature is decreased to 200 K, the device maintains n-type characteristic in the range of −40 to +80 V, but the resistance starts to decrease when the applied gate voltage drops below ~−40 V. This behavior indicates a transition from n-type to p-type occurring in the device during the gate sweeping. Such a transition in the semiconductor characteristics becomes more evident and the turning point moves from the negative toward the positive voltages when the temperature drops further down to 70 K. More interestingly, the resistance shows a plateau-like feature in the range of −40 to +5 V when the temperature decreases further to 40 K. With further decreasing the temperature, the device shows a dominant n-type under a gate voltage from 0 to +80 V at 1.9 K. While for the region range from −80 to −40 V, the device exhibits a prominent bulk p-type. Between these two distinct types is a transition region of −40 to 0 V where both electrons and holes contribute to the device transport. Clearly, based on these experiments, tuning the channel from n-type to p-type becomes achievable by applying a gate voltage. This result is also confirmed by our Hall measurements at 1.9 K, which show a clear type transition when the external voltage changed from 40 to −80 V in Figure 3. Here the total conductance is described as $G_{xy} = (R_{xy})/(R_{xy}^2 + R_s^2)$, where R_{xy} is the Hall resistance and R_s is the sheet resistance. It should be noted that there are competing

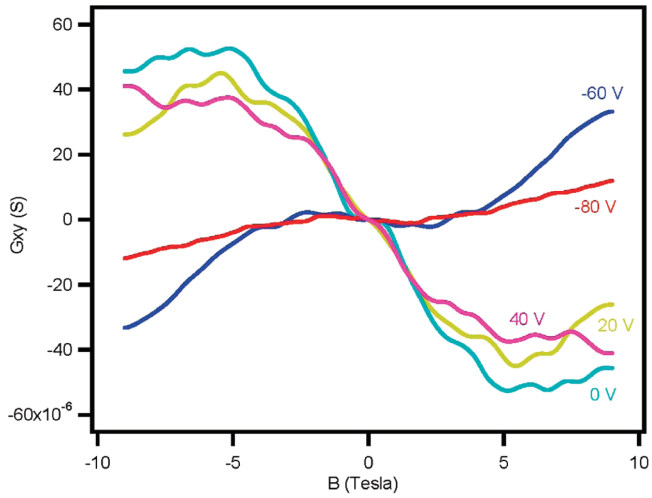

Figure 3. Hall results at different gate voltages, showing a clear type transition from n-type to p-type.

multichannel conductions: surface (electrons) and bulk (electrons and holes). When the contribution from surface electrons and bulk electrons is larger than that from the bulk holes, the system exhibits n-type, like the cases at 0, +20, and +40 V. On the contrary, if the bulk hole conduction dominates, this system will show p-type behavior, that is, at a gate voltage of −60 and −80 V shown in Figure 3. On the basis of these Hall data, we attempted to perform fitting to extract important parameters such as mobility and carrier density. However, due to the complication of multiple channels and external gate involved in this system, we are unable to secure decent fitting results at this stage.

As a powerful method, Shubnikov-de Haas (SdH) oscillations are widely used to investigate the surface states in topological insulators.[14−16] Thus, the gate-controlled SdH oscillations in the Na-doped Bi_2Te_3 nanoplates were carefully investigated. The transport experiments were carried out at low temperature down to 1.9 K with an out-of-plane magnetic field applied to the nanoplates surface. Figure 4a displays the SdH

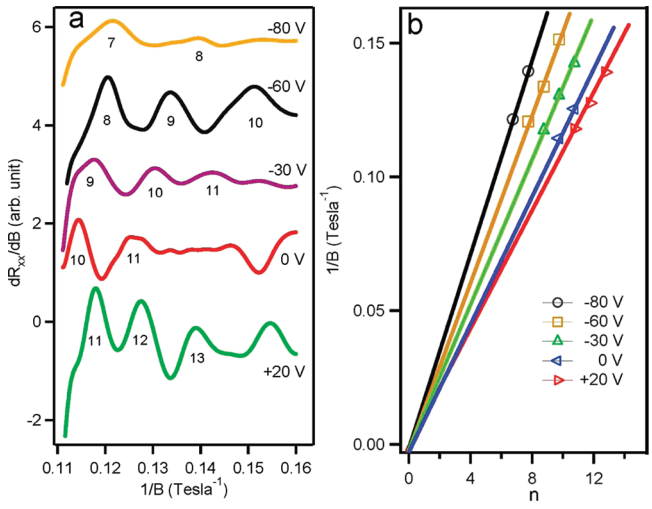

Figure 4. a SdH oscillations under different biases at 1.9 K, which are indexed by particular Landau levels. Note the actual Landau indices should be shifted by −1/4. All curves are vertically offset for clarity. (b) Landau level as a function of $1/B$ under different voltages.

dx.doi.org/10.1021/nl202920p | Nano Lett. 2012, 12, 1170−1175

oscillations under different gate voltages, which exhibit distinct oscillation behaviors from +20 to −80 V. It is known[16] that SdH oscillations are caused by emptying Landau levels with increasing magnetic field and the relationship between the Landau level index n and the magnetic field can be described by $1/B = [(2\pi e\hbar)/(S_F)](n + \gamma)$, where $\hbar$ is the reduced Plank's constant, B is the magnetic flux density, e is the electron charge, the extreme cross-section of the Fermi surface $S_F = \pi k_F^2$, and the Onsager phase $\gamma = 0$ or $1/2$ depending on whether the Berry phase essentially contributes.[16] From the experimental data shown in Figure 3a, linear curves for n and $1/B$ can be obtained by fitting the above equation as all other parameters are constant, as shown in Figure 4b. With the best fitting, we acquired Landau level indices, as marked in Figure 4a. As can be seen, with increasing the gate voltage from −80 to +20 V the frequency of the SdH oscillations becomes larger, and higher Landau levels are reached. The Landau indices are systematically shifted under the different gate biases, indicative of the change of carrier density as well as shifting of the Fermi level (refer to Table 1). It should be noted that the exact Landau level indices should be shifted to the lower level by one-fourth (Supporting Information, Figure S5).[16] The slope of each fitting line is equal to $(2e\hbar)/(k_F^2)$, by which we can obtain the Fermi wavevector, k_F for different gate voltages as summarized in Table 1. In order to extract the cyclotron mass ($m_{cyclotron}$), the SdH amplitudes as a function of temperature are analyzed under the zero voltage (Supporting Information, Figure S6). By fitting the equation $\Delta\sigma_{xx}(T)/\Delta\sigma_{xx}(0) = \lambda(T)/\sinh(\lambda(T))$, where $\lambda(T) = 2\pi^2 k_B T m_{cyclotron}/(\hbar eB)$ and $\Delta\sigma_{xx}$ is the temperature-dependent amplitude of the SdH oscillations, the cyclotron mass ($m_{cyclotron}$) can be estimated to be 0.179 m_0 (m_0 denotes the electron rest mass) under zero gate bias. The fitting result is slightly larger than the existing values for either Bi_2Se_3 (0.16 m_0)[24] or Bi_2Te_3 (0.13 m_0).[14] Note that in Bi_2Se_3, different composition could result in different effective masses,[38] which might explain the discrepancy for our case as additional Na involved in this system. Finally, it is worth mentioning that the cyclotron mass is finite even for a linear energy-band dispersion where the Dirac fermions is massless.[37,39] As reported previously, the cyclotron mass is determined by $m_{cyclotron} = E_F/V_F^2$, which is used to extract the Fermi velocity (V_F).[16,39] With a simple calculation, the Fermi velocity $V_F = (\hbar k_F)/(m_{cyclotron}) = 3.39 \times 10^5$m/s can be determined, which is in the same order as our Bi_2Te_3 nanoribbons[14] and the exfoliated Bi_2Te_3.[16] This result is also consistent with the ARPES measurement of Bi_2Te_3, where a velocity of 4.05×10^5 m/s was determined.[22]

Table 1. Estimated Parameters from the SdH Oscillations at 1.9 K for 20, 0, and −60 V Gate Biases (The Error Is within ±3%)

V_g (V)	n_{2D} (10^{12} cm^{-2})	k_F (Å^{-1})	E_F (meV)	l (nm)	μ (cm^2 V^{-1}s^{-1})
+20	2.29	0.0536	120	96	2705
0	2.19	0.0524	117	119	3439
−60	1.58	0.0445	100	92	3131

As the Dirac-like surface states of Bi_2Te_3 near the Γ point show a linear energy-momentum relationship,[9,14,16] its slope (i.e., V_F) is anticipated to remain unchanged near the Dirac point. Since $E_F = m_{cyclotron}V_F^2 = \hbar k_F V_F$, the Fermi level under different gating conditions can be easily calculated as some shown in Table 1. The calculated parameters from the SdH oscillations are well consistent with the previous results for the surface states reported by Xiu et al.[14] and Qu et al.[16] as well as the ARPES result by Chen et al.,[22] indicating that the SdH oscillations are more likely from the surface states. It is worth to note that only a single obvious period of oscillation was observed in our case under different gate voltages. As the depletion of the bulk carriers can be estimated to be about 12 nm (maximum value, see Supporting Information, Figure S7) and only the bottom surface was tuned given the fact that the nanoplates have a thickness of 35−50 nm, it is reasonable to expect two surfaces' oscillations with different periodicities under a wide range of gate voltages. To address this discrepancy, we note that for our case, the top surface has been exposed in air for a couple of weeks and experienced several photolithographic steps before measurements. It has been reported by Cui group[40] that the Bi_2Se_3 surfaces show strong sign of oxidation after 5 days exposure to air. Likewise, those exposures in our case may have already killed the top surface state, resulting in much less top surface contribution to the whole conduction. As a consequence, the bottom surface plays a major role in the system. On the other hand, if the SdH oscillations originate from bulk, one would expect to see two obvious oscillations with different periodicities when the bulk is tuned from p-type to n-type. Considering the depletion width is about 12 nm (Supporting Information, Figure S7), only the bottom part was tuned. As the top bulk was not tuned, one should be able to see two different oscillation frequencies (from the bottom tuned part and the top untuned part) depending on gate voltages. The fact that only one obvious periodicity was observed in the whole experiments might exclude the possibility of bulk contribution to the SdH oscillations.

Figure 5a is the Fermi level as a function of applied gate voltages for the bottom surface, which delineates a clear trend that the Fermi level raises toward the conduction band with increasing applied gate voltage. Upon a positive voltage engaged, holes are partially depleted from the bulk materials and the Fermi level moves upward; while electrons are depleted when a negative voltage is applied, resulting in the shifting of the Fermi level toward the valence band. To better understand these results, a schematic energy dispersion of Bi_2Te_3 at the Γ point (based on refs 9, 14, and 16.) is presented in Figure 5b, consisting of the valence band, conduction band and linear surface states[9,14,16,22] for the bottom surface. Particularly, the Fermi level is positioned at 117 meV (±3%) above the Dirac point, which is closer to the bulk valence band than the bulk conduction band. However, the system still shows n-type, indicating the dominant electron conductance due to an enhanced surface contribution. Indeed, the Fermi level of n-type Bi_2Te_3 could be closer to the bulk valence band (94 meV above Dirac point) at various doping conditions.[16] Given the fact that holes are the majority carrier in the bulk material when the Fermi level is near the valence band,[41] the surface electrons are anticipated to contribute significantly to the total conductance to ensure the n-type feature of the nanoplates (confirmed later). If we take our previous Bi_2Te_3 nanoribbons[14] as a reference of pure Bi_2Te_3, where no Na was involved, the Fermi level has been lifted up from the valence band toward the middle band gap with the Na doping. We note that the detailed band structure and the nature of Na in Bi_2Te_3 are not clear at the present time and further theoretical as well as experimental studies, such as extended X-ray absorption fine structure, are required. Nevertheless, by doping Na, the Fermi level could be tuned so that the conductance of the bulk contribution is

dx.doi.org/10.1021/nl202920p | Nano Lett. 2012, 12, 1170−1175

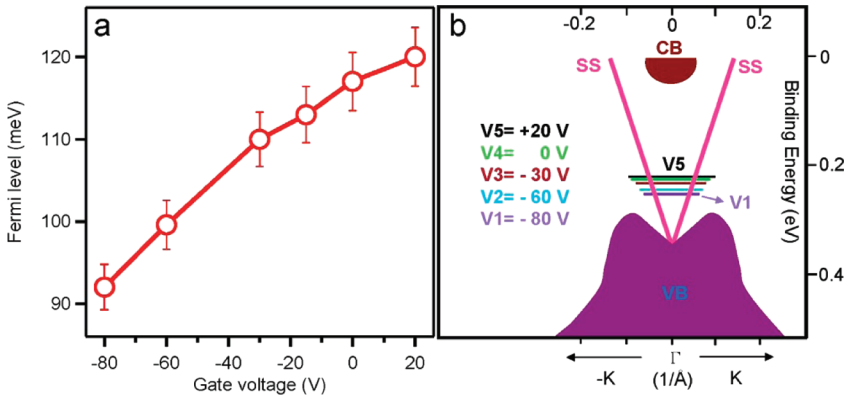

Figure 5. a Fermi level as a function of gate voltage for the bottom surface. b A sketch of the surface state dispersion near the Γ point (traced from refs 16 and 22.) The surface states, valence band and conduction band of the bulk states are denoted as SS, VB and CB, respectively. The Fermi level shifts from the valence band toward the conduction band with increasing gate voltage, resulting in a *p*-type to *n*-type transition.

greatly suppressed, while the surface contribution can be significantly enhanced.

Important parameters such as mean free path and the surface mobility can also be obtained based on these SdH oscillations. Following a well-established approach,[14,16] we estimated transport lifetime of the surface states (τ) by analyzing the Dingle factor[14,16] (Supporting Information, Figure S8). With a simple calculation, one is able to acquire mean free path $l = V_F\tau$ and the surface mobility $\mu = e\tau/m_{cyclotron} = el/\hbar k_F$, and the results are listed in Table 1. Particularly, for $V_g = 0$ V, the calculation yields a mean free path of ~119 nm and a mobility of ~3439 cm^2/V s, which are salient features of surface states: relatively long mean free path and high mobility.

In summary, we demonstrate that gate tunable surface states can be realized in Na-doped Bi_2Te_3 nanoplates and more intriguingly, by applying a back gate, the topological insulators can be tuned from p-type to n-type. Our results are anticipated to trigger further experiments as well as theoretical work in terms of how the amount of Na influences the properties of topological insulators and in what charge states Na exists in the lattice matrix. With controllable surface states, the present results pave the way toward the versatile and practical applications of topological insulators in dissipationless electronic and spintronic devices.

■ ASSOCIATED CONTENT

Supporting Information

Figure S1: The AFM image of a nanoplate and An optical image of a typical fabricated device. Figure S2: $R-T$ curve in a logarithm scale. Figure S3: $\rho-T$ profile. Figure S4:| Typical raw data of R_{xx}. Figure S5: Landau level indices. Figure S6: Temperature-dependent SdH oscillations and cyclotron effective mass. Figure S7: Depletion layer of the bottom surface. Figure S8: Dingle plot analysis. This material is available free of charge via the Internet at http://pubs.acs.org.

■ AUTHOR INFORMATION

Corresponding Author

*E-mail: (Y.W.) yongwang@zju.edu.cn; (J.Z.) j.zou@uq.edu.au; (K.L.W.) wang@ee.ucla.edu

Notes

The authors declare no competing financial interest.

■ ACKNOWLEDGMENTS

We acknowledge the support of the Focus Center Research Program-Center on Functional Engineered Nano Architectonics (FENA), Defense Advanced Research Project Agency (DARPA), the Australia Research Council, National Science Foundation of China (No. 11174244), and UQ Foundation Research Excellence Awards (Y.W.). Y.W. would like to acknowledge helpful discussions with Yabin Fan and Pramey Upadhyaya and experiment support from Li-Te Chang, Caifu Zeng, Sigang Ma, Mingsheng Wang, and Guan Huang from the Device Research Laboratory at UCLA. Y.W. and F.X. designed and fabricated the devices. Y.W., F.X., and L.H. carried out the measurements and analysis. L.C., Z.C., and J.Z. synthesized the Bi_2Te_3 nanoplates and performed the structural analysis. M.L., X.J., J.T., X.K., and X.Y. contributed to the measurements or analysis. K.W and J.Z. supervised the research. Y.W., F.X., K.W., and J.Z. wrote the paper with contribution from L.C.

■ REFERENCES

(1) Bernevig, B. A.; Hughes, T. L.; Zhang, S.-C. *Science* **2006**, *314* (5806), 1757–1761.
(2) Konig, M.; Wiedmann, S.; Brune, C.; Roth, A.; Buhmann, H.; Molenkamp, L. W.; Qi, X.-L.; Zhang, S.-C. *Science* **2007**, *318* (5851), 766–770.
(3) Fu, L.; Kane, C. L.; Mele, E. J. *Phys. Rev. Lett.* **2007**, *98* (10), 106803.
(4) Moore, J. E. *Nature* **2010**, *464* (7286), 194–198.
(5) Franz, M. *Nat. Mater.* **2010**, *9* (7), 536–537.
(6) Peng, H.; Lai, K.; Kong, D.; Meister, S.; Chen, Y.; Qi, X.-L.; Zhang, S.-C.; Shen, Z.-X.; Cui, Y. *Nat. Mater.* **2010**, *9* (3), 225–229.
(7) Manoharan, H. C. *Nat. Nanotechnol.* **2010**, *5* (7), 477–479.
(8) Hasan, M. Z.; Kane, C. L. *Rev. Mod. Phys.* **2010**, *82* (4), 3045.
(9) Zhang, H.; Liu, C.-X.; Qi, X.-L.; Dai, X.; Fang, Z.; Zhang, S.-C. *Nat. Phys.* **2009**, *5* (6), 438–442.
(10) Cho, S.; Butch, N. P.; Paglione, J.; Fuhrer, M. S. *Nano Lett.* **2011**, *11* (5), 1925–1927.
(11) Cheng, P.; Song, C.; Zhang, T.; Zhang, Y.; Wang, Y.; Jia, J.-F.; Wang, J.; Wang, Y.; Zhu, B.-F.; Chen, X.; Ma, X.; He, K.; Wang, L.; Dai, X.; Fang, Z.; Xie, X.; Qi, X.-L.; Liu, C.-X.; Zhang, S.-C.; Xue, Q.-K. *Phys. Rev. Lett.* **2010**, *105* (7), 076801.
(12) Zhang, Y.; He, K.; Chang, C. Z.; Song, C. L.; Wang, L. L.; Chen, X.; Jia, J. F.; Fang, Z.; Dai, X.; Shan, W. Y.; Shen, S. Q.; Niu, Q.; Qi, X. L.; Zhang, S. C.; Ma, X. C.; Xue, Q. K. *Nat. Phys.* **2010**, *6* (8), 584–588.
(13) Xue, Q.-K. *Nat. Nanotechnol.* **2011**, *6* (4), 197–198.

(14) Xiu, F.; He, L.; Wang, Y.; Cheng, L.; Chang, L.-T.; Lang, M.; Huang, G.; Kou, X.; Zhou, Y.; Jiang, X.; Chen, Z.; Zou, J.; Shailos, A.; Wang, K. L. *Nat. Nanotechnol.* **2011**, *6* (4), 216−221.
(15) Ren, Z.; Taskin, A. A.; Sasaki, S.; Segawa, K.; Ando, Y. *Phys. Rev. B* **2010**, *82* (24), 241306.
(16) Qu, D.-X.; Hor, Y. S.; Xiong, J.; Cava, R. J.; Ong, N. P. *Science* **2010**, *329* (5993), 821−824.
(17) Hsieh, D.; Qian, D.; Wray, L.; Xia, Y.; Hor, Y. S.; Cava, R. J.; Hasan, M. Z. *Nature* **2008**, *452* (7190), 970−974.
(18) Qi, X.-L.; Zhang, S.-C. *Phys. Today* **2010**, *63* (1), 33−38.
(19) Hsieh, D.; Xia, Y.; Qian, D.; Wray, L.; Meier, F.; Dil, J. H.; Osterwalder, J.; Patthey, L.; Fedorov, A. V.; Lin, H.; Bansil, A.; Grauer, D.; Hor, Y. S.; Cava, R. J.; Hasan, M. Z. *Phys. Rev. Lett.* **2009**, *103* (14), 146401.
(20) Bianchi, M.; Guan, D.; Bao, S.; Mi, J.; Iversen, B. B.; King, P. D. C.; Hofmann, P. *Nat Commun.* **2010**, *1*, 128.
(21) Xia, Y.; Qian, D.; Hsieh, D.; Wray, L.; Pal, A.; Lin, H.; Bansil, A.; Grauer, D.; Hor, Y. S.; Cava, R. J.; Hasan, M. Z. *Nat. Phys.* **2009**, *5* (6), 398−402.
(22) Chen, Y. L.; Analytis, J. G.; Chu, J.-H.; Liu, Z. K.; Mo, S.-K.; Qi, X. L.; Zhang, H. J.; Lu, D. H.; Dai, X.; Fang, Z.; Zhang, S. C.; Fisher, I. R.; Hussain, Z.; Shen, Z.-X. *Science* **2009**, *325* (5937), 178−181.
(23) Zhang, T.; Cheng, P.; Chen, X.; Jia, J.-F.; Ma, X.; He, K.; Wang, L.; Zhang, H.; Dai, X.; Fang, Z.; Xie, X.; Xue, Q.-K. *Phys. Rev. Lett.* **2009**, *103* (26), 266803.
(24) Butch, N. P.; Kirshenbaum, K.; Syers, P.; Sushkov, A. B.; Jenkins, G. S.; Drew, H. D.; Paglione, J. *Phys. Rev. B* **2010**, *81* (24), 241301.
(25) Chen, X.; Ma, X.-C.; He, K.; Jia, J.-F.; Xue, Q.-K. *Adv. Mater.* **2011**, *23*, 1162−1165.
(26) He, L.; Xiu, F.; Wang, Y.; Fedorov, A. V.; Huang, G.; Kou, X.; Lang, M.; Beyermann, W. P.; Zou, J.; Wang, K. L. *J. Appl. Phys.* **2011**, *109* (10), 103702.
(27) Kong, D.; Randel, J. C.; Peng, H.; Cha, J. J.; Meister, S.; Lai, K.; Chen, Y.; Shen, Z.-X.; Manoharan, H. C.; Cui, Y. *Nano Lett.* **2009**, *10* (1), 329−333.
(28) Hor, Y. S.; Richardella, A.; Roushan, P.; Xia, Y.; Checkelsky, J. G.; Yazdani, A.; Hasan, M. Z.; Ong, N. P.; Cava, R. J. *Phys. Rev. B* **2009**, *79* (19), 195208.
(29) Biswas, R. R.; Balatsky, A. V. *Phys. Rev. B* **2010**, *81* (23), 4.
(30) Taskin, A. A.; Ren, Z.; Sasaki, S.; Segawa, K.; Ando, Y. *Phys. Rev. Lett.* **2011**, *107*, 016801.
(31) Kong, D.; Chen, Y.; Cha, J. J.; Zhang, Q.; Analytis, J. G.; Lai, K.; Liu, Z.; Hong, S. S.; Koski, K. J.; Mo, S.-K.; Hussain, Z.; Fisher, I. R.; Shen, Z.-X.; Cui, Y. *Nat. Nanotechnol.* **2011**, *6* (11), 705−709.
(32) Chen, J.; Qin, H. J.; Yang, F.; Liu, J.; Guan, T.; Qu, F. M.; Zhang, G. H.; Shi, J. R.; Xie, X. C.; Yang, C. L.; Wu, K. H.; Li, Y. Q.; Lu, L. *Phys. Rev. Lett.* **2010**, *105* (17), 176602.
(33) Steinberg, H.; Gardner, D. R.; Lee, Y. S.; Jarillo-Herrero, P. *Nano Lett.* **2010**, *10* (12), 5032−5036.
(34) Hasan, M. Z.; Moore, J. E. *Annu. Rev. Condens. Matter Phys.* **2011**, *2* (1), 55−78.
(35) Checkelsky, J. G.; Hor, Y. S.; Cava, R. J.; Ong, N. P. *Phys. Rev. Lett.* **2011**, *106* (19), 196801.
(36) Choi, J.; Dowben, P. A.; Borca, C. N.; Adenwalla, S.; Bune, A. V.; Ducharme, S.; Fridkin, V. M.; Palto, S. P.; Petukhova, N. *Phys. Rev. B* **1999**, *59* (3), 1819.
(37) Analytis, J. G.; McDonald, R. D.; Riggs, S. C.; Chu, J. H.; Boebinger, G. S.; Fisher, I. R. *Nat. Phys.* **2010**, *6* (12), 960−964.
(38) Analytis, J. G.; Chu, J.-H.; Chen, Y.; Corredor, F.; McDonald, R. D.; Shen, Z. X.; Fisher, I. R. *Phys. Rev. B* **2010**, *81* (20), 205407.
(39) Novoselov, K. S.; Geim, A. K.; Morozov, S. V.; Jiang, D.; Katsnelson, M. I.; Grigorieva, I. V.; Dubonos, S. V.; Firsov, A. A. *Nature* **2005**, *438* (7065), 197−200.
(40) Kong, D.; Cha, J. J.; Lai, K.; Peng, H.; Analytis, J. G.; Meister, S.; Chen, Y.; Zhang, H.-J.; Fisher, I. R.; Shen, Z.-X.; Cui, Y. *ACS Nano* **2011**, *5* (6), 4698−4703.
(41) Sze, S. M.; Ng, K. K. *Physics of Semiconductor Devices*, 3rd ed.; Wiley: New York, 2007.